

## Response letter

We thank Editor's careful consideration of our work. In this rebuttal, we have addressed all the minor concerns raised by the Editor by replying (in black) to your remarks (in blue). The lines numbers in this rebuttal refer to the revised version of the manuscript.

### There are a few minor revisions

#### p11 Need to define $r_s$ ( storage ratio)

**Our reply:** Thank you for pointing this out. In the revised paper, we have explicitly defined the adopted storage width ratio  $r_s$  as: " $r_s = B_s/\bar{B}$  is the storage width ratio between the storage width  $B_s$  and the stream width  $\bar{B}$  that accounts for the effect of storage area (i.e., tidal flats or salt marshes)." See lines 216-218 of the revised manuscript.

#### p14 "This indicates a consistent enhancement of the tidal dynamics...except near ZJ station". This exception needs to be discussed in the paper.

**Our reply:** In the revised paper, we have supplemented the discussion of this point by including the following sentences: "*The exceptional case in ZJ station is likely due to the fact that ZJ station is located near the position of the tidal current limit during the dry season (Guo et al., 2015; Zhang et al., 2018). The shallow and narrow geometry around ZJ station impedes the tidal wave propagation when river discharge increases due to the TGD operation during the dry season (Chen et al., 2012), leading to a remarkably decreasing tidal range in the first half of the year.*" See lines 277-283 of the revised manuscript.

#### p23 Figure 6. The discontinuity in the tidal damping number ( delta) and simulated velocity number in Figure 7needs to be explained.

In a numerical model this behaviour is not acceptable.

**Our reply:** We agree with your comment! In the revise paper, we have explicitly mentioned that "*Here, we used two values for  $K$ :  $K = 80 \text{ m}^{1/3}\cdot\text{s}^{-1}$  in the tide-dominated region ( $x = 0\text{--}32 \text{ km}$ ), and a smaller value of  $K = 55 \text{ m}^{1/3}\cdot\text{s}^{-1}$  in the river-dominated region ( $x = 52\text{--}450 \text{ km}$ ). In addition, to avoid sharp jump in the analytically computed parameters due to the adoption of different friction coefficients, we adopted a friction coefficient of  $K=80\text{--}55 \text{ m}^{1/3}\cdot\text{s}^{-1}$  (indicating a linear reduction of the friction coefficient) over the transitional reach ( $x=32\text{--}52 \text{ km}$ )." See lines 350-355 of the revised manuscript.*

Meanwhile, in section 4.3 of the revised paper, we also explicitly mentioned that "*In Figures 6 and 7, there exist switches of the analytically computed parameters at both ends of the transitional reach ( $x=32\text{--}52 \text{ km}$ ) owing to the change in friction coefficient adopted in the analytical model.*" See lines 402-404 of the revised manuscript.

### References:

Chen, J., Wang, Z., Li, M., Wei, T. and Chen, Z.: Bedform characteristics during

falling flood stage and morphodynamic interpretation of the middle–lower Changjiang (Yangtze) River channel, China, *Geomorphology*, 147, 18-26, <https://10.1016/j.geomorph.2011.06.042>, 2012.

Guo, L., van der Wegen, M., Jay, D.A., Matte, P., Wang, Z.B., Roelvink, D., and He, Q.: River-tide dynamics: Exploration of nonstationary and nonlinear tidal behavior in the Yangtze River Estuary, *J. Geophys. Res.*, 120(5), 3499-3521, <https://10.1002/2014JC010491>, 2015.

Zhang, F., Sun, J., Lin, B., and Huang, G.: Seasonal hydrodynamic interactions between tidal waves and river flows in the Yangtze Estuary, *J. Marine Syst.*, 186, 17-28, <https://doi.org/10.1016/j.jmarsys.2018.05.005>, 2018.

1           **Impacts of Three Gorges Dam’s operation on spatial-temporal**  
2           **patterns of tide-river dynamics in the Yangtze River estuary, China**

3   Huayang Cai<sup>1,2,3,4</sup>, Xianyi Zhang<sup>1,2,3</sup>, Leicheng Guo<sup>4</sup>, Min Zhang<sup>5,\*</sup>, Feng Liu<sup>1,2,3</sup>,  
4   Qingshu Yang<sup>1,2,3</sup>

5  
6   *1. Institute of Estuarine and Coastal Research, School of Marine Engineering and*  
7   *Technology, Sun Yat-sen University, Guangzhou, China*

8   *2. Guangdong Provincial Engineering Research Center of Coasts, Islands and Reefs,*  
9   *Guangzhou, China*

10   *3. Southern Marine Science and Engineering Guangdong Laboratory (Zhuhai),*  
11   *Zhuhai, China*

12   *4. State Key Laboratory of Estuarine and Coastal Research, East China Normal*  
13   *University, Shanghai, China*

14   *5. Shanghai Normal University, School of Environmental and Geographical Sciences,*  
15   *Shanghai, China*

16   **Corresponding author:** Min Zhang

17   **Corresponding author’s E-mail:** zhangmin@shnu.edu.cn  
18

19   **Key points**

20   1. Impacts of TGD operation on tide-river dynamics are quantified using an  
21   analytical model.

22   2. The strongest impacts occurred during autumn and winter due to the seasonal  
23   freshwater regulation by TGD.

24   3. The alteration of tide-river dynamics may exert considerable impacts on  
25   sustainable water resource management in dam-controlled estuaries.

设置了格式: 上标

设置了格式: 上标

设置了格式: 上标

30

31

32

33 **Abstract**

34 The Three Gorges Dam (TGD), located in the mainstream of the Yangtze River, is the  
35 world's largest hydroelectric station in terms of installed power capacity. It was  
36 demonstrated that the TGD had caused considerable modifications in the downstream  
37 freshwater discharge due to its seasonal operation mode of multiple utilisation for  
38 flood control, irrigation, and power generation. To understand the impacts of the  
39 freshwater regulation of TGD, an analytical model is adopted to explore how the  
40 operation of TGD may affect the spatial-temporal patterns of tide-river dynamics in  
41 the Yangtze River estuary. We evaluated the effect of TGD by comparing the changes  
42 in major tide-river dynamics in the post-TGD period (2003–2014) with those in the  
43 pre-TGD period (1979–1984). The results indicate that the strongest impacts occurred  
44 during the autumn and winter, corresponding to a substantial reduction in freshwater  
45 discharge during the wet-to-dry transition period and slightly increased discharge  
46 during the dry season. The underlying mechanism leading to changes in the tide-river  
47 dynamics lies in the alteration of freshwater discharge, while the impact of geometric  
48 change is minimal. Overall, the results suggest that the spatial-temporal pattern of  
49 tide-river dynamics is sensible to the freshwater regulation of the TGD, so that the  
50 ecosystem function of the estuary may undergo profound disturbances. The results  
51 obtained from this study can be used to set scientific guidelines for water resource

52 management (e.g. navigation, flood control, salt intrusion) in dam-controlled estuarine  
53 systems.

54 **Key words:** seasonal freshwater regulation, Three Gorges Dam, analytical model,  
55 tide-river dynamics, Yangtze River estuary

## 56 **1. Introduction**

57 Estuaries are transition zones where river meets ocean (Savenije, 2012). Tide-river  
58 interactions, a result of both hydrologic drivers and geomorphic constraints, are  
59 highly dynamic in estuaries (Buschman et al., 2009; Sassi and Hoitink, 2013; Guo et  
60 al., 2015; Cai et al., 2016; Hoitink and Jay, 2016; Hoitink et al., 2017; Du et al., 2018).

61 In natural conditions, they usually experience a wide range of temporal variations, in  
62 timescale ranging from a fortnight to season (e.g. Zhang et al., 2018). Human  
63 intervention, such as dam construction in the upstream parts of a river and the  
64 growing number of water conservancy projects built along large rivers (such as  
65 freshwater withdrawal), have caused seasonal changes in downstream freshwater  
66 discharge delivery, leading to adjustments in the function of fluvial and estuarine  
67 hydrology (e.g. Lu et al., 2011; Mei et al., 2015; Dai et al., 2017). Consequently, it is  
68 important to understand the impacts of large-scale human intervention, such as flood  
69 control, navigation, salt intrusion, and freshwater withdrawal, which are relevant not  
70 only to tide-river dynamics and riparian ecology but also to sustainable water resource  
71 management in general.

72

73 River discharge generally fluctuates following a wet-dry cycle due to the seasonal

74 variation of precipitation in the upstream river basin. For instance, the Yangtze River,  
75 the largest river in China in terms of mean discharge, which flows into the East China  
76 Sea, has a maximum river discharge during summer in July and a low value during  
77 winter in January, with a maximum discharge difference of approximately 38,000  
78 m<sup>3</sup>/s (Cai et al., 2016). Similar seasonal variations are also identified in other large  
79 rivers in eastern and southern Asia, such as the Mekong River in Vietnam, Ganges  
80 River in India, and Pearl River in China, under the influence of a monsoon climate.  
81 However, most large rivers have been significantly dammed at the central and upper  
82 reaches in recent decades, dramatically modifying stream hydrology and sediment  
83 delivery, resulting in changes in hydraulics and river delta development trend at the  
84 lower reaches (e.g. Räsänen et al, 2017; Rahman et al., 2018; Liu et al., 2018). Due to  
85 the fact that the response of tide-river interactions to the impacts of dams are diverse  
86 and non-uniform and that many more dams are to be built in the future, the impacts of  
87 the hydrodynamic interactions between tidal waves and seasonal river flows from  
88 natural variations and anthropogenic activities have become a common focus in  
89 international hydraulic research, especially in large tidal rivers.

90

91 The Yangtze River estuary, located near the coastal area of East China Sea, is one of  
92 the largest estuaries in Asia. In the mouth of the Yangtze River estuary, bifurcation  
93 occurs and the characteristics of tides have been broadly investigated in previous  
94 studies (e.g. Zhang et al., 2012; Lu et al., 2015; Alebregtse and Swart, 2016).  
95 However, in these studies, river influences are usually neglected. In recent years, the

96 processes of nonlinear interactions between tidal wave and river flow in the Yangtze  
97 River estuary have received increasing attention (e.g. Guo et al., 2015; Zhang et al.,  
98 2015a, b; Cai et al., 2016; Kuang et al., 2017; Zhang et al., 2018). However, recent  
99 studies on tidal properties, such as asymmetry, changes near the mouth area, and  
100 seasonal variations in tidal wave propagation and fluvial effects over the entire 600  
101 km of the tidal river, up to the tidal limit of the Datong hydrological station, have  
102 been limited. In addition, the operation of the Three Gorges Dam (TGD), the largest  
103 dam in the world, has substantially affected the downstream river hydrology and  
104 sediment delivery. There is a variety of debate regarding the potential impacts of TGD  
105 on the downstream river morphology, hydrology, and ecology, since the underlying  
106 mechanism of the impact of the TGD is not fully understood. Specifically, the TGD  
107 operation has altered the downstream fluvial discharge and water levels on the  
108 seasonal scale, directly following the reservoir seasonal impounding and release of  
109 water volume (e.g. Chen et al., 2016; Guo et al., 2018). However, the impacts of  
110 seasonal freshwater regulation by the TGD on the spatial-temporal tide-river  
111 dynamics in the downstream estuarine area have not been systematically investigated.  
112 For example, during the dry season TGD operation increased the multi-year monthly  
113 averaged river discharge at Datong station from  $9520 \text{ m}^3 \cdot \text{s}^{-1}$  to  $12896 \text{ m}^3 \cdot \text{s}^{-1}$  in  
114 January, while during wet season the regulation reduced the river discharge from  
115  $49900 \text{ m}^3 \cdot \text{s}^{-1}$  to  $44367 \text{ m}^3 \cdot \text{s}^{-1}$  in July during the pre- and post- TGD period.

116

117 In this study, for the first time, the spatial-temporal variations in the hydrodynamic

118 processes due to the interactions of tidal flow and fluvial discharge in the Yangtze  
119 River estuary caused by natural forcing and human intervention were studied, with  
120 specific focus on the effect of TGD seasonal regulation. Here, we adopted a  
121 well-developed analytical model proposed by Cai et al. (2014a, 2016) to investigate  
122 the spatial-temporal patterns of tide-river dynamics in the entire Yangtze River estuary  
123 and quantify the impacts of the TGD operation. In the following sections, we  
124 introduce the study site of the Yangtze River estuary. This is followed by a description  
125 of the available data and analytical model of tide-river dynamics in Section 3.  
126 Subsequently, we applied the model to the Yangtze River estuary, where the TGD has  
127 operated since 2003 (Section 4). In particular, we explored the alteration of the  
128 tide-river dynamics after the TGD closure and summarise the impacts of the TGD on  
129 the spatial-temporal patterns of tide-river dynamics. The impacts of channel geometry  
130 and river discharge alterations on tide-river dynamics as well as the implications for  
131 sustainable water resource management were then discussed in Section 5. Finally,  
132 some key findings were addressed in Section 6.

133

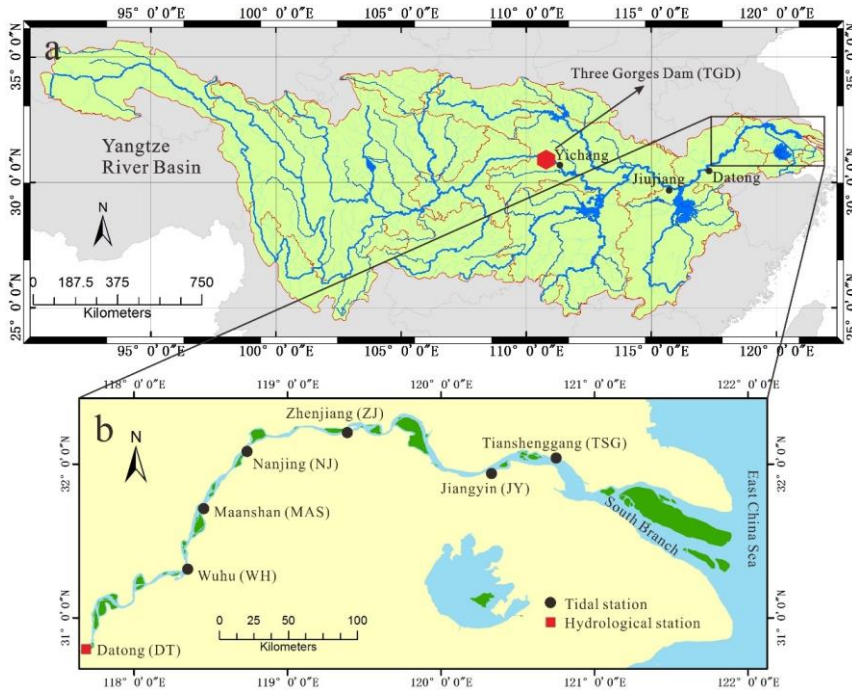
## 134 **2. Overview of the Yangtze River estuary**

135 The Yangtze River, flowing from west to east in central China, is one of the world's  
136 most important rivers due to its great economic and social relevance. It has a length of  
137 about 6300 km and a basin area of about 190,000 km<sup>2</sup> (Figure 1a). The Yangtze River  
138 basin is geographically divided into three parts, the upper, central, and lower  
139 sub-basins, and contains an estuary area with partitions at Yichang, Jiujiang, and

140 Datong (DT), respectively (Figure 1a). Of concern in this study are the impacts of the  
141 Three Gorges Dam (TGD), the world's largest dam, on the spatial-temporal patterns of  
142 tide-river dynamics in the estuarine area. It is located about 45 km upstream of  
143 Yichang (Figure 1a). The TGD project began in 2003; by 2009, when full operations  
144 began, the total water storage capacity rose up to  $\sim 40 \text{ km}^3$ , equivalent to 5% of the  
145 Yangtze's annual discharge. Downstream the DT station, where the tidal limit is  
146 located, the Yangtze River estuary extends  $\sim 630 \text{ km}$  to the seaward end of the South  
147 Branch. Wuhu (WH), Maanshan (MAS), Nanjing (NJ), Zhenjiang (ZJ), Jiangyin (JY),  
148 and Tianshenggang (TSG) are the major gauging stations along the mainstream in the  
149 seaward direction (Figure 1b). Under the control of the Asian monsoon climate, river  
150 discharges show distinct seasonal patterns. In 1979–2012, more than 70% of  
151 freshwater was discharged at DT occurred during summer (May–October).

152

153 Apart from river flows, tidal waves are also recognised as the major sources of energy  
154 for hydrodynamics in the Yangtze River estuary, which is characterised by a meso-tide  
155 with a tidal range of up to 4.6 m and a mean tidal range of  $\sim 2.7 \text{ m}$  near the estuary  
156 mouth. According to the observation in the Gaoqiaoju tidal gauging station (1950–  
157 2012), the averaged ebb tide duration (7.5 h) is a bit longer than the averaged flood  
158 tide duration (5 h), indicating an irregular semidiurnal character (Zhang et al., 2012).



159  
 160 Figure 1. Maps of the Yangtze River basin (a) and Yangtze River estuary (b) with the  
 161 location of tidal gauging and hydrological stations shown with black solid circles and  
 162 red solid rectangles.

163  
 164 **3. Data and Methodology**

165 **3.1 Source of Data**

166 To quantitatively investigate the relationship between freshwater discharge regulation  
 167 caused by the TGD operation and the tide-river dynamics, monthly averaged  
 168 hydrological data for both pre-TGD (1979–1984) and post-TGD (2003–2014) periods  
 169 of tidal range and water level from the above-mentioned six tidal gauging stations  
 170 along the Yangtze River estuary were collected. They were published by the Yangtze

171 Hydrology Bureau of the People's Republic of China. The monthly averaged tidal  
 172 amplitude is determined by averaging the daily difference between high and low  
 173 water levels and dividing by two. To correctly quantify the residual water level along  
 174 the Yangtze estuary, locally measured water level at different gauging stations are  
 175 corrected to the national mean sea level of Huanghai 1985.

176

### 177 **3.2 Analytical model for tide-river dynamics**

#### 178 **3.2.1 Basic equations**

179 In tidal rivers, the tidally averaged water level (i.e. residual water level) depicts a  
 180 steady gradient, which usually increases with freshwater discharge (e.g. Sassi and  
 181 Hoitink, 2013). The key to deriving the dynamics of the residual water level lies in the  
 182 one-dimensional momentum equation, which can be expressed as (e.g. Savenije, 2005,  
 183 2012):

$$184 \quad \frac{\partial U}{\partial t} + U \frac{\partial U}{\partial x} + g \frac{\partial Z}{\partial x} + \frac{gh}{2\rho} \frac{\partial \rho}{\partial x} + g \frac{U|U|}{K^2 h^{4/3}} = 0, \quad (1)$$

185 where  $U$  is the cross-sectional averaged velocity,  $Z$  is the free surface elevation,  $h$  is  
 186 the water depth,  $g$  is the acceleration due to gravity,  $t$  is the time,  $\rho$  is the water density,  
 187  $x$  is the longitudinal coordinate directed landward, and  $K$  is the Manning-Strickler  
 188 friction coefficient. It was demonstrated that in the subtidal momentum balance, the  
 189 residual water level slope is primarily balanced by the residual friction term (Vignoli  
 190 et al., 2003; Buschman et al., 2009; Cai et al., 2014a, for a detailed derivation, readers  
 191 can refer to the Appendix A):

$$192 \quad \frac{\partial Z}{\partial x} = - \frac{U|U|}{K^2 h^{4/3}} \quad (2)$$

193

194 where the overbars indicate the tidal average. For a single channel with the residual  
195 water level set to 0 at the estuary mouth (i.e.  $\bar{Z} = 0$  at  $x = 0$ ), the integration of

196 Equation (2)(2)(2) leads to an analytical expression for the residual water level

$$197 \quad \bar{Z}(x) = -\int_0^x \frac{\partial \bar{Z}}{\partial x} = -\int_0^x \frac{U|U|}{K^2 h^{4/3}}. \quad (3)$$

198 To derive the analytical solutions for tide-river dynamics, we assume that the  
199 longitudinal variation of cross-sectional area  $\bar{A}$  and width  $\bar{B}$  can be described by the  
200 following exponential functions (see also Toffolon et al., 2006; Cai et al., 2014a):

$$201 \quad \bar{A} = \bar{A}_r + (\bar{A}_0 - \bar{A}_r) \exp\left(-\frac{x}{a}\right), \quad (4)$$

$$202 \quad \bar{B} = \bar{B}_r + (\bar{B}_0 - \bar{B}_r) \exp\left(-\frac{x}{b}\right), \quad (5)$$

203 where  $\bar{A}_0$  and  $\bar{B}_0$  represent the tidally averaged cross-sectional area and width at the  
204 estuary mouth, respectively,  $\bar{A}_r$  and  $\bar{B}_r$  represent the asymptotic riverine  
205 cross-sectional area and width, respectively, and  $a$  and  $b$  are the convergence lengths  
206 of the cross-sectional area and width, respectively. The advantage of these equations  
207 for approximating the shape of the estuary is that they account not only for the  
208 exponential shape in the lower part of the tidal river but also for the approximately  
209 prismatic channel in the upstream part of the tidal river. We further assume a nearly  
210 rectangular cross-section, considering a large width to depth ratio; hence, the tidally  
211 averaged depth is given by  $\bar{h} = \bar{A}/\bar{B}$  and the cross-sectional area variability can be  
212 primarily attributed to the change in depth.

### 213 3.2.2 Analytical solution for tidal hydrodynamics

设置了格式: 字体颜色: 文字 1

设置了格式: 字体颜色: 文字 1

214 It was shown by Cai et al. (2014a, b, 2016) that the tide-river dynamics is dominantly  
 215 controlled by four dimensionless parameters (see their definitions in Table 1). They  
 216 include: the dimensionless tidal amplitude  $\zeta$  (representing the boundary condition in  
 217 the seaward side), the estuary shape number  $\gamma$  (representing the cross-sectional area  
 218 convergence), the friction number  $\chi$  (representing the bottom frictional effect), and the  
 219 dimensionless river discharge  $\varphi$  (representing the impact of freshwater discharge).  
 220 The definitions of these four variables are defined in Table 1, where  $\eta$  is the tidal  
 221 amplitude,  $v$  is the velocity amplitude,  $U_r$  is the river flow velocity,  $\omega$  is the tidal  
 222 frequency,  $r_{s, \bar{B}} = B_s / \bar{B} r_s$  is the storage width ratio between the storage width  $B_s$   
 223 and the stream width  $\bar{B}$  that accounts for the effect of storage area (i.e., tidal flats or  
 224 salt marshes) is the storage width ratio accounting for the effect of storage area (i.e.  
 225 tidal flats or salt marshes), and  $c_0$  is the classical wave celerity defined as  
 226  $c_0 = \sqrt{g\bar{h}/r_s}$ .

227 Table 1. Definitions of dimensionless parameters used in the analytical model

Local variables	Dependent variables
Dimensionless tidal amplitude $\zeta = \eta / \bar{h}$	Amplification number $\delta = c_0 d\eta / (\eta \omega d x)$
Estuary shape number $\gamma = c_0 (\bar{A} - \bar{A}_r) / (\omega a \bar{A})$	Velocity number $\mu = v / (r_s \zeta c_0) = v \bar{h} / (r_s \eta c_0)$
Friction number $\chi = r_s g c_0 \zeta [1 - (4\zeta / 3)^2]^{-1} / (\omega K^2 \bar{h}^{4/3})$	Celerity number $\lambda = c_0 / c$
Dimensionless river discharge	Phase lag

- 设置了格式: 字体颜色: 文字 1, 英语(英国)
- 设置了格式: 字体: 非倾斜, 字体颜色: 文字 1, 英语(英国)

---

$$\varphi = U_r / v$$

---

$$\varepsilon = \pi / 2 - (\phi_z - \phi_U)$$

---

228

229 In this study, we used the analytical solutions proposed by Cai et al. (2014a, b, 2016),  
230 in which the solutions of the major tide-river dynamics are derived by solving a set of  
231 four implicit equations for the tidal damping, the velocity amplitude, the wave celerity,  
232 and the phase lag (see details in Appendix B). The major dependent parameters can be  
233 described by the following four variables (see also Table 1):  $\delta$  represents the  
234 damping/amplification number describing the increase ( $\delta > 0$ ), or decrease ( $\delta < 0$ ) of  
235 the tidal wave amplitude along the estuary axis,  $\mu$  represents the velocity number  
236 indicating the ratio of actual velocity amplitude to the frictionless value in a prismatic  
237 channel,  $\lambda$  represents the celerity number representing the classical wave celerity  $c_0$   
238 scaled by the actual wave celerity  $c$ , and  $\varepsilon$  represents the phase lag between the high  
239 water (HW) and high water slack (HWS) or between the low water (LW) and low  
240 water slack (LWS). It is important to note that the phase lag (ranging between 0 and  
241  $\pi/2$ ) is a key parameter in classifying the estuary, where  $\varepsilon = 0$  suggests the tidal wave  
242 is featured by a standing wave, while  $\varepsilon = \pi/2$  indicates a progressive wave. For a  
243 simple harmonic wave, the phase lag is defined as  $\varepsilon = \pi / 2 - (\phi_z - \phi_U)$ , where  $\phi_z$  and  
244  $\phi_U$  are the phases of elevation and current, respectively (Savenije, et al., 2008).

245

### 246 **3.2.3 Analytical solution for the entire channel**

247 It is worth noting that the analytically computed tide-river dynamics  $\mu$ ,  $\delta$ ,  $\lambda$ , and  $\varepsilon$  only  
248 represent local hydrodynamics since they depend on local (fixed position) values of

249 the dimensionless parameters, i.e. the tidal amplitude  $\zeta$ , the estuary shape number  $\gamma$ ,  
250 the friction number  $\chi$ , and the river discharge  $\varphi$  (see Table 1). To correctly reproduce  
251 the tide-river dynamics for the entire channel, a multi-reach technique is adopted by  
252 subdividing the entire estuary into multiple reaches to account for the longitudinal  
253 variations of the estuarine sections (e.g. bed elevation, bottom friction). For a given  
254 tidal damping/amplification number  $\delta$  and tidal amplitude  $\eta$  at the seaward boundary,  
255 it is possible to determine the tidal amplitude at a distance  $\Delta x$  (e.g. 1 km) upstream by  
256 simple explicit integration. Hence, the analytical solution for the entire channel can be  
257 obtained by step-wise integration in this way.

258

## 259 **4. Results**

### 260 **4.1 Observational analysis on the alteration of tide-river dynamics after TGD** 261 **closure**

262 To quantify the impacts of TGD operation on the downstream tide-river dynamics, we  
263 divided the time series into two periods, including a pre-TGD period (1979–1984,  
264 representing the condition before the operation of the TGD) and a post-TGD period  
265 (2003–2014, after the closure of the TGD with an operating TGD). Figure 2 shows the  
266 changes in the observed tidal range  $\Delta H$  and residual water level  $\Delta \bar{Z}$  before and after  
267 the closure of the TGD at the six gauging stations, together with the change in  
268 freshwater discharge  $\Delta Q$  observed at the DT hydrological station. Figure 2 and Table  
269 2 clearly show that the monthly averaged river discharge in January, February, and  
270 March substantially increased by 35.5%, 30.5%, and 16.4%, respectively, due to the

271 considerable release of freshwater from the TGD. On the other hand, we observe a  
272 significant decrease in freshwater discharge in September, October, and November,  
273 decreasing by 20.1%, 33.2%, and 20.8%, respectively. The reason can be primarily  
274 attributed to the impounding water of the TGD during these months, especially in  
275 October. During the other months, the impacts of TGD on the change in the  
276 freshwater discharge are relatively small, mimicking the natural condition before the  
277 operation of the TGD.

278

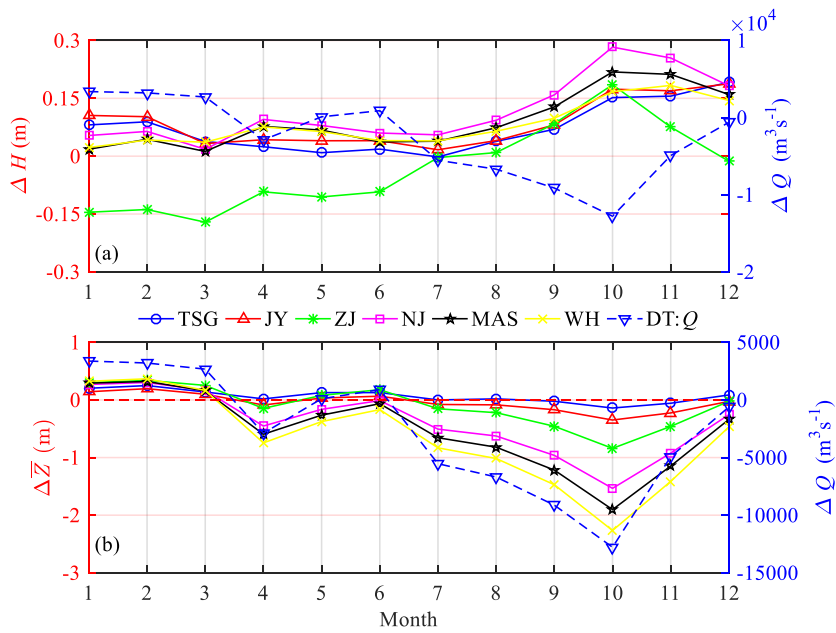
279 In Figure 2a we observe an increasing trend in tidal range for the post-TGD period at  
280 the six gauging stations, except for the marked decrease at the ZJ station in the first  
281 half of the year (i.e. January–June). On average, the maximum increase (0.20 m) in  
282 tidal range occurs in October, which is mainly due to the substantial reduction of river  
283 discharge caused by the TGD operation. This indicates a consistent enhancement of  
284 tidal dynamics along the Yangtze estuary, except the reach near the ZJ station. The  
285 exceptional case in ZJ station is likely due to the fact that ZJ station is located near the  
286 position of the tidal current limit during the dry season (Guo et al., 2015; Zhang et al.,  
287 2018). The shallow and narrow geometry around ZJ station impedes the tidal wave  
288 propagation when river discharge increases due to the TGD operation during the dry  
289 season (Chen et al., 2012), leading to a remarkably decreasing tidal range in the first  
290 half of the year.

291

292 –For the residual water level, Figure 2b clearly shows that the change in the residual

设置了格式: 字体: 非倾斜

293 water level directly follows that of the river discharge due to the stable relationship  
 294 between these two parameters. In particular, we see that the residual water levels  
 295 increased by 0.26 m, 0.30 m, and 0.16 m, respectively, in January, February, and  
 296 March, while they significantly decreased by 0.72 m, 1.17 m, and 0.70 m, respectively,  
 297 in September, October, and November. In addition, the decrease trend in residual  
 298 water level is more significant at upstream stations when compared with those in the  
 299 downstream areas.



300  
 301 Figure 2. Changes in monthly averaged (a) tidal range  $\Delta H$  and (b) residual water level  
 302  $\Delta \bar{Z}$  together with the freshwater discharge  $\Delta Q$  along the Yangtze River estuary.

303  
 304  
 305

306

307

308

309

310 Table 2. Comparison of multi-year monthly averaged river discharge  $Q$  ( $\text{m}^3 \cdot \text{s}^{-1}$ )

311 between the pre-TGD and the post-TGD periods

Month	1	2	3	4	5	6	7	8	9	10	11	12
Pre-TGD	9520	10527	16298	25050	30867	38283	49900	47276	45317	38467	23633	14810
Post-TGD	12896	13733	18974	22165	30971	39180	44367	40590	36187	25682	18714	14203
Change	3376	3206	2675	-2885	105	896	-5533	-6687	-9130	-12784	-4919	-607

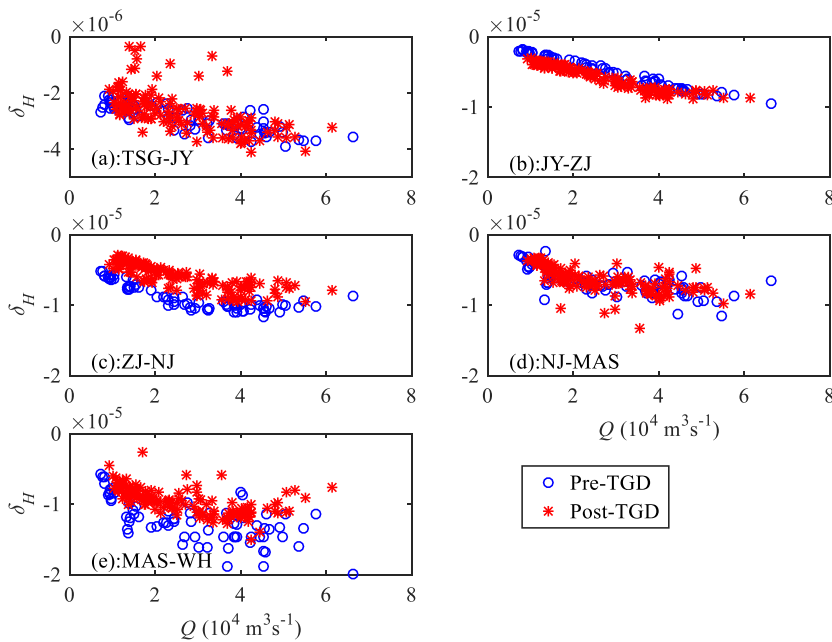
312 Since the TGD operation affects tide-river dynamics primarily through the alteration  
313 of the freshwater discharge, it is worth exploring the patterns of trends in the  
314 relationship between the freshwater discharge and gradients of the main tidal  
315 parameters with respect to distance (i.e. the tidal damping rate and the residual water  
316 level slope). Here, we estimated the tidal damping rate  $\delta_H$  and the residual water level  
317 slope  $S$  for a reach of  $\Delta x$  by using the following expressions:

$$318 \quad \delta_H = \frac{1}{(H_1 + H_2)/2} \frac{H_2 - H_1}{\Delta x}, \quad (6)$$

$$319 \quad S = \frac{\bar{Z}_2 - \bar{Z}_1}{\Delta x}, \quad (7)$$

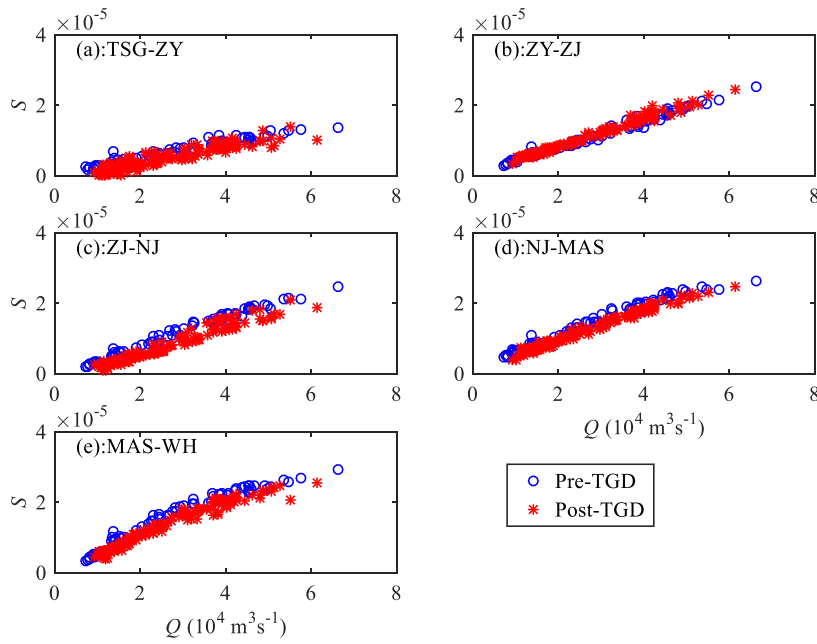
320 where  $H_1$  and  $\bar{Z}_1$  are the tidal amplitude and residual water level on the seaward side,  
321 respectively, whereas  $H_2$  and  $\bar{Z}_2$  are the corresponding values  $\Delta x$  upstream,  
322 respectively. Figure 3 presents the computed tidal damping rates for different reaches  
323 along the Yangtze estuary based on the observed tidal ranges at the six gauging

324 stations. It is remarkable that the tidal damping rates at the ZJ-NJ and MAS-WH  
 325 reaches have significantly increased during the post-TGD period, which suggests an  
 326 enhancement of tidal dynamics under the current freshwater discharge conditions. On  
 327 the contrary, a noticeable decrease in  $\delta_H$  was observed at the JY-ZJ reach, which  
 328 corresponds to a decrease in tidal range at the ZJ station for the low river discharge  
 329 conditions (from January to May, see Figure 2a). At TGS-JY and NJ-MAS, no  
 330 significant change in  $\delta_H$  is observed. In Figure 4, a consistent decrease in the residual  
 331 water level slope  $S$  is observed along the Yangtze estuary, except for the JY-ZJ reach.  
 332 This means that the residual friction effect becomes weaker in the post-TGD period  
 333 since the residual water level slope is primarily balanced by the residual friction term  
 334 (Cai et al., 2014a, b, 2016).



335  
 336 Figure 3. Changes in tidal damping rate  $\delta_H$  before and after the TGD closure for

337 different reaches along the Yangtze estuary: (a) TGS-JY, (b) JY-ZJ, (c) ZJ-NJ, (d)  
 338 NJ-MAS, (e) MAS-WH.



339  
 340 Figure 4. Changes in residual water level slope  $S$  before and after the TGD closure for  
 341 different reaches along the Yangtze estuary: (a) TGS-JY, (b) JY-ZJ, (c) ZJ-NJ, (d)  
 342 NJ-MAS, (e) MAS-WH.

343

#### 344 4.2 Performance of the analytical model reproducing the tide-river dynamics

345 The analytical model presented in Section 3.2 was subsequently applied to the  
 346 Yangtze River estuary, with the seaward boundary using the tidal amplitude imposed  
 347 at the TSG station and the landward boundary using the river discharge imposed at the  
 348 DT station. The computation length of the estuary is 470 km, covering the entire  
 349 estuary from TSG to DT. The adopted geometric characteristics (including the tidally

350 averaged cross-sectional area, width, and depth) are the same for both pre- and  
351 post-TGD periods, which were extracted from a digital elevation model (DEM) using  
352 Yangtze River estuary navigation charts surveyed in 2007. The geometric  
353 characteristics, calibrated by fitting the observed values using Equations (4) and (5),  
354 are presented in Table 3, where a relatively large cross-sectional area convergence  
355 length ( $a = 151$  km) is evident, with a relatively small width ( $b = 44$  km), indicating a  
356 fast transition from a funnel-shaped reach to a prismatic reach in terms of width. It is  
357 worth noting that the Yangtze River estuary is characterised by a typical semidiurnal  
358 character; thus, a typical  $M_2$  tidal period (i.e. 12.42 h) was adopted in the analytical  
359 model. For the sake of simplification, we assume that the storage width ratio  $r_S = 1$ .  
360 Hence, the only calibrated parameter is the Manning-Strickler friction coefficient  $K$ .  
361 Here, we used two values for  $K$ :  $K = 80 \text{ m}^{1/3} \cdot \text{s}^{-1}$  in the tide-dominated region ( $x = 0$ –  
362 42–32 km), and a smaller value of  $K = 55 \text{ m}^{1/3} \cdot \text{s}^{-1}$  in the river-dominated region  
363 ( $x = 4252$ –450 km). In addition, to avoid sharp jump in the analytically computed  
364 parameters due to the adoption of different friction coefficients, we adopted a friction  
365 coefficient of  $K=80$ – $55 \text{ m}^{1/3} \cdot \text{s}^{-1}$  (indicating a linear reduction of the friction coefficient)  
366 over the transitional reach ( $x=32$ – $52$  km).

设置了格式: 字体: 非倾斜

设置了格式: 字体: 非倾斜

设置了格式: 字体: 非倾斜

367  
368 The analytically computed results were compared with the observed tidal amplitudes  
369 and the residual water levels at five gauging stations along the Yangtze estuary  
370 (Figure 5). It can be seen that the overall correspondence between analytical results  
371 and observations is good, with high coefficients of determination ( $R^2 > 0.95$ ), which

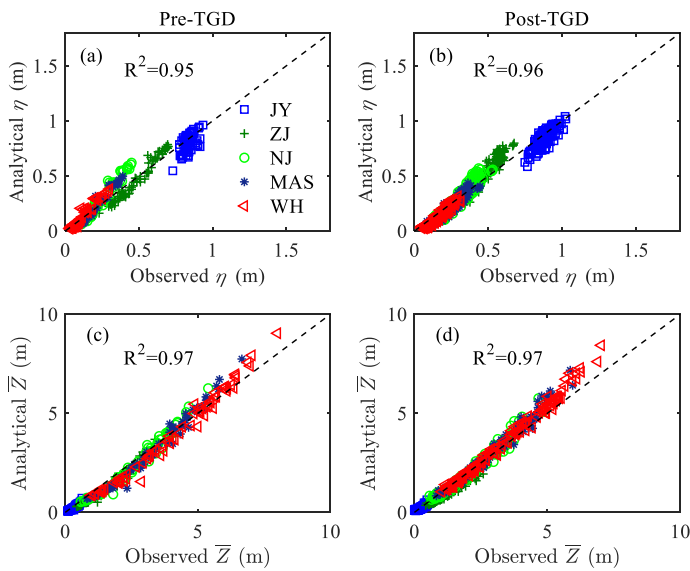
372 suggests the usefulness of the present analytical model for reproducing the tide-river  
 373 dynamics, given the gross features of flow characteristics and estuarine geometry.

374  
 375  
 376  
 377

378 Table 3. Characteristics of geometric parameters in the Yangtze River estuary

Characteristics	River	Mouth	Convergence length $a/b$ (km)
Cross-sectional area $\bar{A}$ (m <sup>2</sup> )	12,135	51,776	151
Width $\bar{B}$ (m)	2005	6735	44

379



380

381 Figure 5. Comparison of monthly averaged values for (a, b) analytically computed

382 tidal amplitude  $\eta$  and (c, d) residual water level  $\bar{Z}$  against the observations in the  
383 Yangtze River estuary for the pre-TGD period (1979–1984) and post-TGD period  
384 (2003–2014).

385

386

387

### 388 **4.3 Impacts of TGD operation on spatial-temporal patterns of tide-river** 389 **dynamics**

390 With the significant seasonal discharge variations resulting from the TGD regulation,  
391 an understanding of the seasonal impacts on tide-river dynamics along the estuary has  
392 become increasingly important. In Figures 6 and 7, we see how the TGD operation  
393 impacts the longitudinal variation of the main tidal dynamics in terms of the four  
394 dependent parameters  $\delta$ ,  $\lambda$ ,  $\mu$ , and  $\varepsilon$  for different seasons. The most considerable  
395 changes in the major tide-river dynamics occurred in both autumn and winter seasons,  
396 which correspond to the substantial reduction in freshwater discharge in the  
397 wet-to-dry transition period (i.e. autumn) and slightly increased freshwater discharge  
398 in the dry season (i.e. winter) due to the TGD operation since 2003 (see Table 2). On  
399 the other hand, the impacts of the TGD operation on the tide-river dynamics during  
400 the spring and summer are relatively minor due to the negligible change in the  
401 freshwater discharge. However, we do notice that the TGD had exerted slight  
402 influence on tide-river dynamics in the downstream reaches ( $x < 250$  km) during the  
403 summer, with the maximum freshwater discharge occurring within a year. In addition,

404 it appears that there exists a critical position corresponding to the maximum tidal  
405 damping (or minimum value of  $\delta$ ) upstream in which the tidal damping becomes weak.  
406 This phenomenon occurs particularly in the spring, summer, and autumn. The  
407 underlying mechanism is elaborated in the discussion section.

408

409 Figures 6a, c, e, g show the comparison of the analytically computed tidal damping  
410 number  $\delta$  before and after the closure of the TGD, in which we clearly observe that  
411 the longitudinal tidal damping effect was considerably weakened in autumn, while it  
412 was slightly enhanced in winter after the TGD closure. This was expected since  
413 freshwater discharges tend to dampen the tidal wave primarily through the  
414 enhancement of the friction term (Horrevoets et al., 2004; Cai et al., 2014a, b, 2016).

415 Figures 6b, d, g, i show a similar picture for the wave celerity number  $\lambda$ , which is  
416 positively correlated to the tidal damping number  $\delta$ , according to the celerity equation  
417 (11) in Appendix B. Figure 7 shows the longitudinal computation of the velocity  
418 number  $\mu$  and the phase lag  $\varepsilon$  for both periods. The impacts of the TGD operation on  
419 the velocity scale and phase lag are similar to the tidal damping, i.e. the larger the

420 freshwater discharge, the smaller the velocity number and the phase lag. In Figures 6  
421 and 7, there exist switches of the analytically computed parameters at both ends of the  
422 transitional reach ( $x=32-52$  km) owing to the change in friction coefficient adopted in  
423 the analytical model.

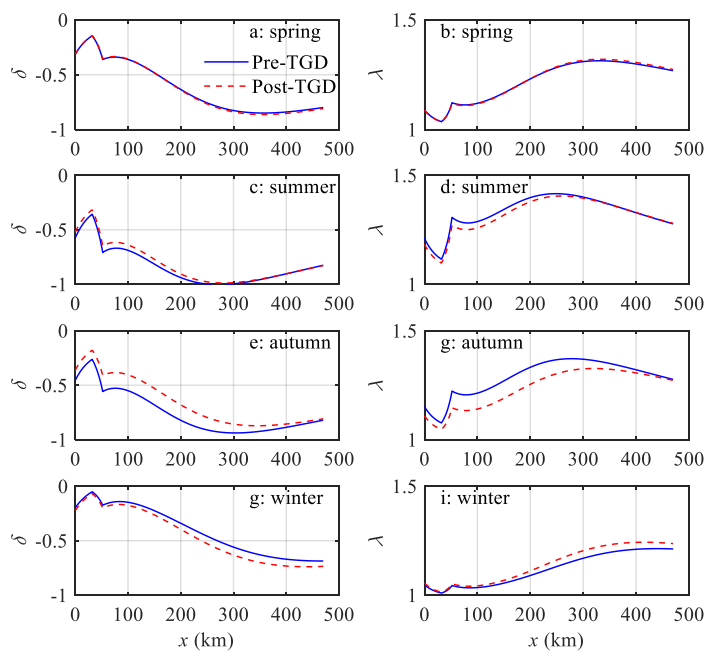
424

425 Overall, in the seaward reach of the estuary, the effect of freshwater discharge

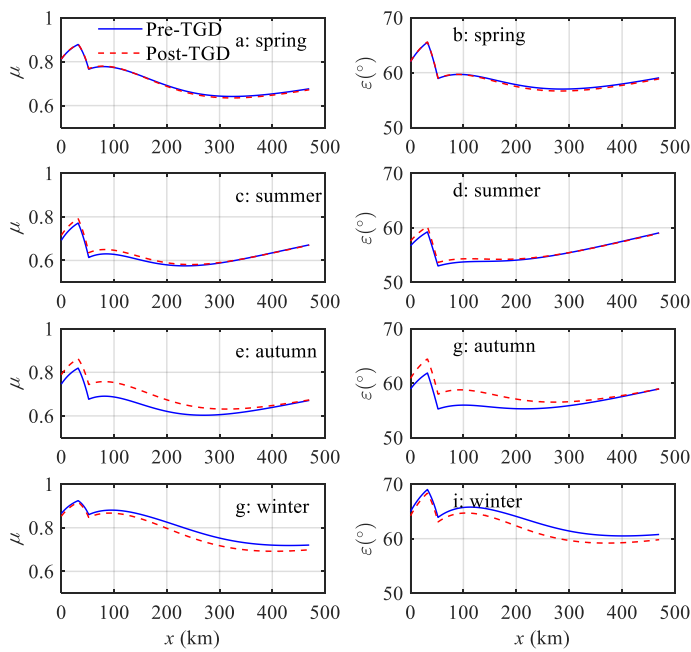
设置了格式: 字体: 非倾斜

设置了格式: 字体: 非倾斜

426 alteration by the TGD operation on the major tide-river dynamics (i.e.  $\delta$ ,  $\lambda$ ,  $\mu$ , and  $\varepsilon$ )  
 427 was less significant because of the small ratio of freshwater discharge to tidal  
 428 discharge. On the other hand, in the upstream reach of the estuary, the changes in the  
 429 four dependent parameters are also small due to the substantial tidal attenuation as a  
 430 result of the long-distance propagation from the estuary mouth. Therefore, the pattern  
 431 of seasonal variation due to the TGD operation is relatively small at both ends of the  
 432 estuary, whereas the largest variation usually occurs in the middle reach of the estuary.  
 433 This finding was supported by the results of harmonic analysis using the numerical  
 434 results (Zhang et al., 2018). Similar phenomena have also been identified in other  
 435 large fluvial meso-tide estuaries, such as the Mekong River estuary and Amazon  
 436 River estuary, where dam operation altered the seasonal patterns of tide-river  
 437 dynamics (Kosuth et al., 2009; Hecht et al., 2018).  
 438



439 Figure 6. Longitudinal variability of simulated tidal damping number  $\delta$  (a, c, e, g) and  
 440 celerity number  $\lambda$  (b, d, g, i) along the Yangtze estuary in different seasons (spring: a,  
 441 b; summer: c, d; autumn: e, g; winter: g, i) for both the pre-TGD and the post-TGD  
 442 periods.



443  
 444 Figure 7. Longitudinal variability of simulated velocity number  $\mu$  (a, c, e, g) and phase  
 445 lag  $\epsilon$  (b, d, g, i) along the Yangtze estuary in different seasons (spring: a, b; summer: c,  
 446 d; autumn: e, g; winter: g, i) for both the pre-TGD and the post-TGD periods.

447

## 448 5. Discussion

### 449 5.1 The impact of channel geometry alteration on tide-river dynamics

450 Dam operations, which dramatically modified downstream flow and sediment

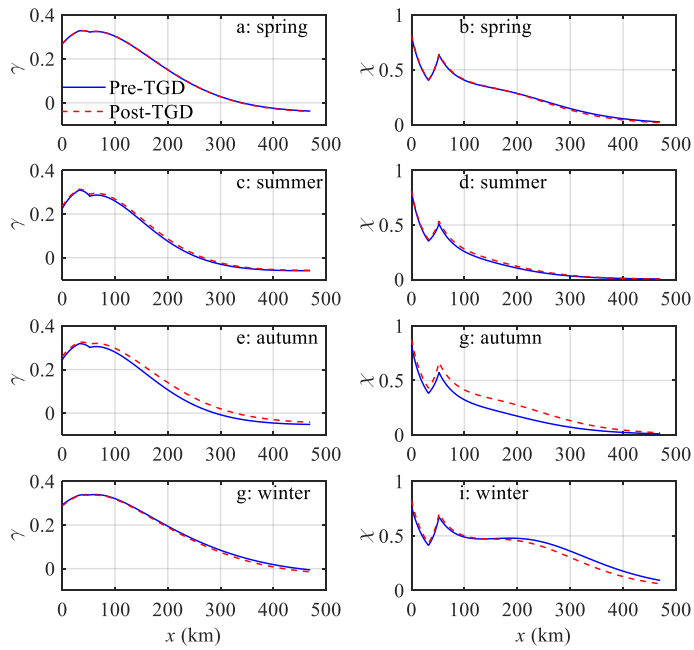
451 regimes, are becoming an increasingly important factor controlling the morphological  
452 evolution. Previous studies show that, as a result of the trapping of sediments by the  
453 TGD, considerable erosion occurred in the first several hundred km downstream of  
454 the TGD, considerably coarsening the bedload (Yang et al., 2014). In particular, the  
455 river bed immediately downstream was eroded at a rate of 65 Mt/yr in 2001–2002  
456 (Yang et al., 2014). It was shown by Lyu et al. (2018) that due to a dramatic reduction  
457 in the sediment discharge following the construction of the TGD, a significant change  
458 in size, geometry, and spatial distribution of pool-riffles occurred downstream;  
459 however, this adjustment was limited to the reaches close to the TGD. It should be  
460 noted that the bathymetry adopted in the analytical model is restricted to the estuarine  
461 area in 2007, which is only 4 years after the TGD closure in 2003, and it is before the  
462 full operation of the TGD began in 2009. In addition, the TGD is around 1600 km  
463 away from the estuary mouth, and its influence on the estuarine morphology normally  
464 has a lag effect of at least 4–5 years, as discussed by Wang et al. (2008). Hence, the  
465 adopted geometry has been only partly altered after the TGD closure. The  
466 morphological change of Yangtze Estuary can be even more profound in recent years  
467 due to the continuous and accumulated impact from the TGD. Further adjustment of  
468 morphological change due to the sedimentation in the TGD could exert a considerable  
469 impact on the tide-river dynamics in the estuarine region (e.g., Du et al., 2018; Shaikh  
470 et al., 2018). Further study on the impact of morphological adjustment on the  
471 tide-river dynamics is required in the future.

472

473 **5.2 The impact of freshwater discharge alteration on tide-river dynamics**

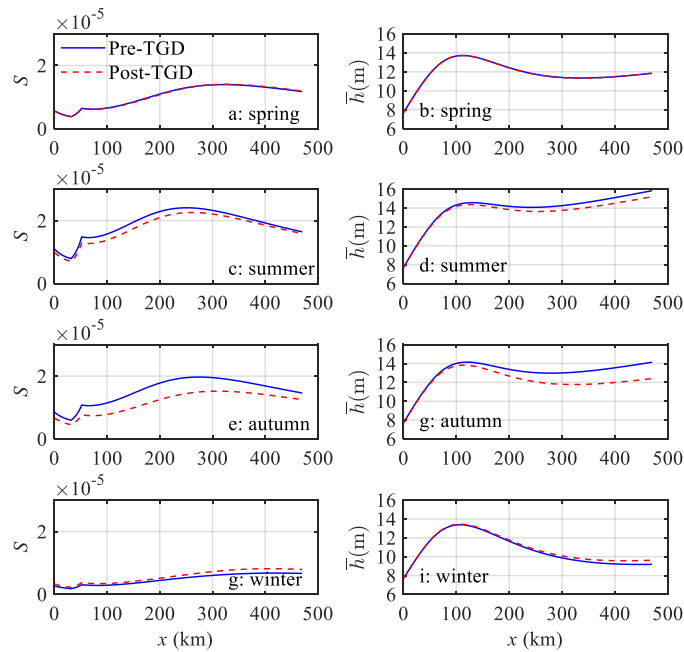
474 The water conservancy of the TGD has multiple purposes, in which the seasonal  
475 discharge regulation and their impact on the ecosystem are well documented (e.g. Mei  
476 et al., 2015a, b; Chen et al., 2016; Guo et al., 2018). However, the actual influence of  
477 discharge regulation on the river-tide dynamics in the estuarine area is not fully  
478 understood. With the analytical reproduction of tide-river dynamics for pre- and  
479 post-TGD periods, it is possible to quantify the extent of the changes in the major  
480 tidal dynamics, including the estuary shape number  $\gamma$  and friction number  $\chi$  (Figure 8),  
481 and the residual water level slope  $S$  and water depth  $h$  (Figure 9) along the Yangtze  
482 River estuary. In general, during the transition from the wet season (summer–autumn)  
483 to the dry season (winter–spring), the water level and corresponding fluvial discharge  
484 downstream from the TGD is first raised by the impounding water and then reduced  
485 by the release of water, which would substantially change the tide-river dynamics in  
486 the downstream estuarine area, with the maximum variation occurring in autumn and  
487 the minimum variation occurring in spring.

488



489

490 Figure 8. Longitudinal variability of simulated estuary shape number  $\gamma$  (a, c, e, g) and  
 491 friction number  $\chi$  (b, d, g, i) along the Yangtze estuary in different seasons (spring: a,  
 492 b; summer: c, d; autumn: e, g; winter: g, i) for both the pre-TGD and the post-TGD  
 493 periods.



494

495 Figure 9. Longitudinal variability of simulated residual water level slope  $S$  (a, c, e, g)  
 496 and water depth  $\bar{h}$  (b, d, g, i) along the Yangtze estuary in different seasons (spring: a,  
 497 b; summer: c, d; autumn: e, g; winter: g, i) for both the pre-TGD and the post-TGD  
 498 periods.

499

500 Figures 8 and 9 show that during the wet season (summer–autumn), the estuary shape  
 501 number  $\gamma$  and friction number  $\chi$  experience a general increase, while a decrease in the  
 502 residual water level slope  $S$  and water depth  $\bar{h}$  can be identified in the post-TGD  
 503 period due to the reduction in freshwater discharge. However, the changes in these  
 504 major dynamics vary significantly along the channel. Near the estuary mouth, where  
 505 tidal influence overwhelms the influence from freshwater discharge, the difference is

506 relatively small, as the magnitude of the freshwater discharge is small when compared  
507 with that of the tidal discharge. Meanwhile at the upstream reach of the estuary, where  
508 the riverine influence dominates that of the tide, the difference is also small due to the  
509 attenuation of the tidal wave propagation over a long distance. Consequently, the most  
510 significant changes in major tide-river dynamics occurred in the middle reach of the  
511 Yangtze River estuary due to the discharge regulation of the TGD during the wet  
512 season. By contrast, during the dry season (winter–spring), especially in winter, the  
513 opposite trend was observed, indicating a slight increase in  $\gamma$  and  $\chi$ , and a slight  
514 decrease in  $S$  and  $\bar{h}$  due to the additional release of discharge from the TGD. In  
515 addition, we also observed that the changes in tide-river dynamics caused by the TGD  
516 operation were much stronger upstream than in the lower stream.

517

### 518 **5.3 Implications for water resource management**

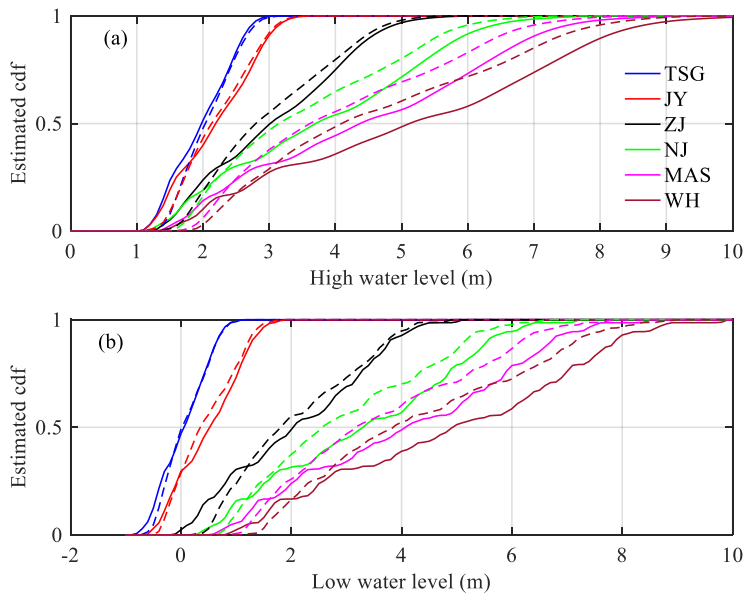
519 The construction of the TGD is the largest hydro-development project ever performed  
520 in the world, having multiple influences on downstream water resource management,  
521 including navigation, flood control, tidal limit variation, and salt intrusion.

522

#### 523 **5.3.1 Implications for navigation**

524 The navigation condition is mainly controlled by both high water and low water levels.  
525 Figure 10 shows the estimation of the cumulative distribution function (cdf) for both  
526 the high-water level (Figure 10a) and the low-water level (Figure 10b) at the six  
527 gauging stations along the Yangtze River estuary for both the pre- and post-TGD

528 periods. The results indicate that navigation conditions during the non-flood season  
529 are generally improved, because both percentages of high-water and low-water levels  
530 are increased due to the additional freshwater discharge released from the TGD. On  
531 the other hand, during the flood season, the reduction in the freshwater discharge by  
532 TGD impounding tends to exert a negative impact on navigation. However, the  
533 reduced freshwater discharges in the late summer and autumn are not of sufficient  
534 magnitude to cause any navigation problems. This is due to the fact that the mean  
535 water levels during the flood season are relatively high; hence, the regulating flow  
536 quantity and regulating capacity are relatively small (e.g. Chen et al., 2016). In  
537 general, due to the staggered regulation in freshwater discharge, seasonally, the actual  
538 navigation condition is improved due to the significant increase in the percentage of  
539 low water levels.



540

541 Figure 10. Cumulative distribution function (cdf) estimated by using the kernel  
542 smoothing function (a) for high water level and (b) low water level at six gauging  
543 stations along the Yangtze estuary. The solid lines represent the pre-TGD period,  
544 while the dashed lines represent the post-TGD period.

545

### 546 **5.3.2 Implications for flood control**

547 Flood control is one of the most important functions of building dams and reservoirs  
548 in large rivers. Before the construction of the TGD, the Yangtze River basin suffered  
549 from frequent and disastrous flood threats. For instance, the floods of 1998 in the  
550 Yangtze River were reported to have killed 3656 people, destroyed 5.7 million homes,  
551 and damaged seven million more. Many studies have examined the flood control  
552 capacity of the TGD over the past two decades (Zhao et al., 2013; Chen et al., 2014).  
553 In particular, the capability of the TGD flood control is influenced by multiple factors  
554 (e.g. Huang et al., 2018), particularly in the estuarine area, which is strongly  
555 influenced by tides from the ocean. During the flood season, the reduced freshwater  
556 discharge by TGD impounding benefits the flood control by reducing the peak flood  
557 discharge. However, as the tidal influence is enhanced, both the percentages of high  
558 water and low water levels for the post-TGD period are considerably increased, as  
559 shown in Figure 10, indicating a decreased flood control capability. For instance, at  
560 the WH gauging station located in the upstream part of the Yangtze River estuary, the  
561 8-m high-water level increased by approximately 10% after the TGD closure during  
562 the wet season. The corresponding flood prevention standard, therefore, is reduced  
563 due to the increased high-water level (see also Nakayama and Shankman, 2013).

564

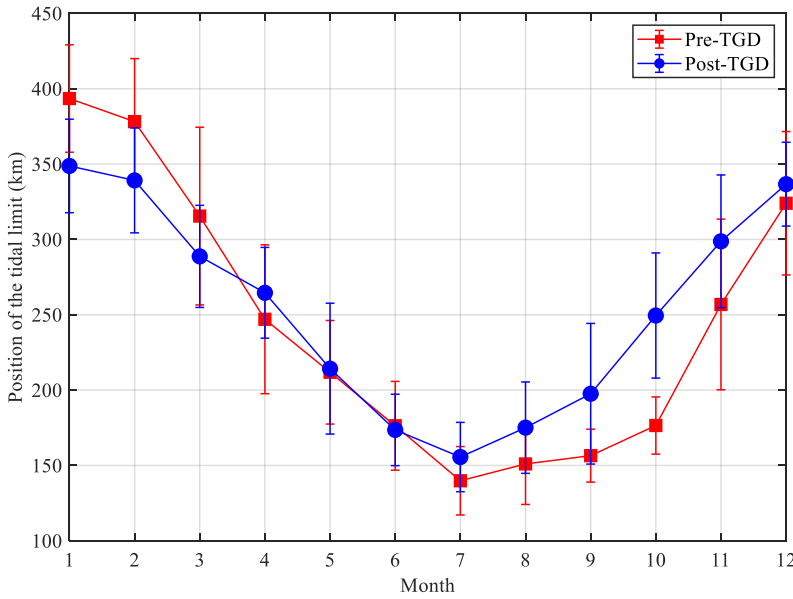
### 565 **5.3.3 Implications for tidal limit**

566 It is important to detect the position of the tidal limit (corresponding with the position  
567 where the tidal amplitude to depth ratio is less than a certain threshold, e.g.  $\frac{\eta}{h} < 0.02$ ),  
568 which is the farthest point upstream where a river is affected by tidal fluctuations,  
569 since it is essential for surveying, navigation, and fisheries management, in general  
570 (e.g. Shi et al., 2018). Subsequently, we are able to define the tide-influenced length  
571 as the distance upstream from the estuary mouth to the tidal limit. Generally, the tidal  
572 limit fluctuates with the changes in the seasonal freshwater discharges. Field  
573 measurements have demonstrated that tidal limit can reach as far as the NJ station and  
574 further upstream during the dry season, while during the wet season, it is pushed  
575 down to the ZJ station and may be pushed further downward to the JY station under  
576 spate conditions. Figure 11 shows the analytically computed tidal limit position for  
577 both the pre- and post-TGD periods. It can be observed that the tidal limit moved  
578 downstream by about 45 km and 39 km in January and February under the impact of  
579 the additional release of discharge from TGD during the dry season. During the  
580 transition from dry to wet seasons (January–May), the total freshwater discharge from  
581 TGD increases, and we identify further downstream movement of the tidal limit,  
582 although to a smaller extent. The reverse of the post-TGD tidal limit in April is due to  
583 the decrease in the freshwater discharge compared with the pre-TGD tidal limit (see  
584 Table 2). The TGD storage period begins in June, and the tidal limit moved upstream  
585 by a large amount compared with the pre-TGD period. The largest change occurred  
586 during October when the tidal limit moved from 175 km pre-TGD to 250 km

587 post-TGD due to the substantial increase in freshwater discharge (see Table 2).

588

589



590

591 Figure 11. Temporal variation of the position of the tidal limit relative to the TSG  
592 station for both the pre-TGD and the post-TGD periods. The vertical error bar at each  
593 data point indicates the standard deviation of the analytically computed time series.

594

#### 595 5.3.4 Implications for salt intrusion

596 The operation of the TGD changed the location of tidal limit, which, in turn, directly  
597 influences the intensity of saltwater intrusion, especially during the dry season, when  
598 the freshwater discharge is low and saltwater intrusion is important (e.g. Cai et al.,  
599 2015). The analysis of tide-river dynamics shows that the tidal dynamics are

600 considerably enhanced during the autumn due to the substantial decline in freshwater  
601 discharged into the estuary, which may lead to enhanced saltwater intrusion. However,  
602 with supplemented discharge after the TGD during the winter, saltwater intrusion  
603 tends to be significantly suppressed, and the isohalines are pushed seaward by  
604 additional river discharges (e.g. An et al., 2009; Qiu and Zhu, 2013). In contrast,  
605 during the wet season, the TGD operation slightly extended the timing of saltwater  
606 intrusion and increased its intensity by impounding freshwater. Since the total river  
607 discharge rate during the wet season is the largest during the year, the influence of  
608 saltwater on freshwater reservoirs along the coastal area is limited. Therefore, the  
609 operation of TGD is overall favourable for reducing the burden of freshwater  
610 supplement in the tidally influenced estuarine areas. However, to quantify the  
611 potential impacts of TGD's operation on salt intrusion and related aquatic ecosystem  
612 health in general, it is required to couple the hydrodynamic model to the ecological or  
613 salt intrusion model (e.g., Qiu and Zhu, 2013; Cai et al., 2015).

614

## 615 **6. Conclusions**

616 An analytical approach was used to examine the potential impacts of TGD operation  
617 on the spatial-temporal patterns of tide-river dynamics along the Yangtze River  
618 estuary. It was shown that the freshwater regulation caused by the TGD, on a seasonal  
619 scale, exerts significant impacts on the tide-river dynamics, with the maximum  
620 influence occurring in autumn and winter. This generally corresponds to a dramatic  
621 decrease in freshwater discharge during the wet-to-dry transition period and a slight

622 increase in discharge during the dry season. The analytical results indicate that the  
623 discharge regulation by the TGD drives the alterations in the tide-river dynamics  
624 instead of the geometric change. In particular, the change in the freshwater discharge  
625 changes the estuary shape number (representing the geometric effect), the residual  
626 water level slope (representing the effective frictional effect) and, hence, the tide-river  
627 dynamics. This study, using the Yangtze River estuary as an example, provides an  
628 effective yet simple method to quantify the seasonal regulation in freshwater  
629 discharge by large reservoirs or dams on hydrodynamics in estuaries. The results  
630 obtained from this study will, hopefully, shed new light on aspects of water resource  
631 management, such as navigation, flood control, and salt intrusion.

632

633 **Data availability.** Data and results are available from the authors upon request.

634 **Author contributions.** All authors contributed to the design and development of the  
635 work. The experiments were originally carried out by Huayang Cai. Xianyi Zhang and  
636 Leicheng Guo carried out the data analysis. Min Zhang built the model and wrote the  
637 paper. Feng Liu and Qingshu Yang reviewed the paper.

638 **Competing interests.** The authors declare that they have no conflict of interest.

639 **Acknowledgments.** We acknowledge the financial support from the National Key  
640 R&D of China (Grant No. 2016YFC0402600), from the Open Research Fund of State  
641 Key Laboratory of Estuarine and Coastal Research (Grant No. SKLEC-KF201809),  
642 from the National Natural Science Foundation of China (Grant No. 51709287 and  
643 41701001), and from the Guangdong Provincial Natural Science Foundation of China

644 (Grant No. 2017A030310321).

645

646 **References**

647 An, Q., Wu., Y., and Taylor, S.: Influence of the Three Gorges Project on saltwater  
648 intrusion in the Yangtze River Estuary, *Environ. Geol.*, 56, 1679-1686,  
649 <https://doi.org/10.1007/s00254-008-1266-4>, 2009.

650 Alebregtse, N. C., and de Swart, H. E.: Effect of river discharge and geometry on  
651 tides and net water transport in an estuarine network, an idealized model applied to  
652 the Yangtze estuary, *Cont. Shelf. Res.*, 123, 29-49, [https://doi.org/10.1016/  
653 j.csr.2016.03.028](https://doi.org/10.1016/j.csr.2016.03.028), 2016.

654 Buschman, F. A., Hoitink, A. J. F., van der Vegt, M., and Hoekstra, P.: Subtidal water  
655 level variation controlled by river flow and tides, *Water Resour. Res.*, 45(10), W10420,  
656 <https://doi.org/10.1029/2009WR008167>, 2009.

657 Cai, H., Savenije, H. H. G., and Toffolon, M.: Linking the river to the estuary,  
658 influence of river discharge on tidal damping, *Hydrol. Earth Syst. Sci.*, 18(1), 287-304,  
659 <https://doi.org/10.5194/hess-18-287-2014>, 2014a.

660 Cai, H., Savenije, H. H. G., and Jiang, C.: Analytical approach for predicting fresh  
661 water discharge in an estuary based on tidal water level observations, *Hydrol. Earth  
662 Syst. Sci.*, 18(10), 4153-4168, <https://doi.org/10.5194/hess-18-4153-2014>, 2014b.

663 Cai, H., Savenije, H.H.G., Zuo, S., Jiang, C., and Chua, V.: A predictive model for salt  
664 intrusion in estuaries applied to the Yangtze estuary, *J. Hydrol.*, 529, 1336-1349,  
665 <https://doi.org/10.1016/j.jhydrol.2015.08.050>, 2015.

666 Cai, H., Savenije, H. H. G., Jiang, C. Zhao L., Yang Q.: Analytical approach for  
667 determining the mean water level profile in an estuary with substantial fresh water  
668 discharge, *Hydrol. Earth Syst. Sci.*, 20, 1-19, <https://doi.org/10.5194/hess-20-1-2016>,  
669 2016.

670 Chen, J., Finlayson, B.L., Wei, T., Sun, Q., Webber, M., Li, M., and Chen, Z.:  
671 Changes in monthly flows in the Yangtze River, China-With special reference to the  
672 Three Gorges Dam, *J. Hydrol.*, 536, 293-301, [https://doi.org/10.1016/j.jhydrol.](https://doi.org/10.1016/j.jhydrol.2016.03.008)  
673 [2016.03.008](https://doi.org/10.1016/j.jhydrol.2016.03.008), 2016.

674 [Chen, J., Wang, Z., Li, M., Wei, T. and Chen, Z.: Bedform characteristics during](#)  
675 [falling flood stage and morphodynamic interpretation of the middle-lower](#)  
676 [Changjiang \(Yangtze\) River channel, China, \*Geomorphology\*, 147, 18-26,](#)  
677 <https://10.1016/j.geomorph.2011.06.042>, 2012.

678 Chen, J., Zhong, P.A., Zhao, Y.F.: Research on a layered coupling optimal operation  
679 model of the Three Gorges and Gezhouba cascade hydropower stations, *Energy*  
680 *Convers. Manage.* 86 (5), 756–763, <https://doi.org/10.1016/j.enconman.2014.06.043>,  
681 2014.

682 Dai, M., Wang, J., Zhang, M., and Chen, X.: Impact of the Three Gorges Project  
683 operation on the water exchange between Dongting Lake and the Yangtze River, *Int. J.*  
684 *Sediment Res.*, 32, 506-514, <https://doi.org/10.1016/j.ijsrc.2017.02.006>, 2017.

685 Dronkers, J. J.: *Tidal Computations in River and Coastal Waters*, Elsevier, New York,  
686 USA, <https://doi.org/10.1126/science.146.3642.390>, 1964.

687 Du, J., Shen, J., Zhang, Y.J., Ye, F., Liu, Z., Wang, Z., Wang, Y.P., Yu, X., Sisson, M.,

688 Wang, H.V.: Tidal Response to Sea-Level Rise in Different Types of Estuaries: The  
689 Importance of Length, Bathymetry, and Geometry, *Geophys Res Lett.*, 45(1), 227-235,  
690 <https://doi.org/10.1002/2017GL075963>, 2018.

691 Friedrichs, C. T., and Aubrey, D. G.: Non-linear tidal distortion in shallow well-mixed  
692 estuaries, A synthesis, *Estuar. Coast. Shelf S.*, 27, 521-545,  
693 [https://doi.org/10.1016/0272-7714\(88\)90082-0](https://doi.org/10.1016/0272-7714(88)90082-0), 1988.

694 Guo, L., van der Wegen, M., Jay, D.A., Matte, P., Wang, Z.B., Roelvink, D.J.A., He,  
695 Q.: River-tide dynamics, Exploration of nonstationary and nonlinear tidal behavior in  
696 the Yangtze River estuary, *J. Geophys. Res.*, 120(5), 3499-3521,  
697 <https://doi.org/10.1002/2014JC010491>, 2015.

698 Guo, L., Su, N., Zhu, C., and He, Q.: How have the river discharges and sediment  
699 loads changed in the Changjiang River basin downstream of the Three Gorges Dam? *J.*  
700 *Hydrol.*, 560, 259-274, <https://doi.org/10.1016/j.jhydrol.2018.03.035>, 2018.

701 [Guo, L., van der Wegen, M., Jay, D.A., Matte, P., Wang, Z.B., Roelvink, D., and He,](#)  
702 [Q.: 2015. River-Tide Dynamics: Exploration of Nonstationary and Nonlinear](#)  
703 [Tidal Behavior in the Yangtze River Estuary, J. Geophys. Res., 120\(5\), 3499-3521,](#)  
704 <https://10.1002/2014JC010491>, 2015.

705 Hoitink, A. J. F., and Jay, D. A.: Tidal river dynamics: implications for deltas, *Rev.*  
706 *Geophys.*, 54, 240-272, <https://doi.org/10.1002/2015RG000507>, 2016.

707 Hoitink, A. J. F., Wang, Z. B., Vermeulen, B., Huismans, Y., and Kastner, K.: Tidal  
708 controls on river delta morphology, *Nat. Geosci.*, [https://doi.org/10,](https://doi.org/10.1038/ngeo3000)  
709 10.1038/ngeo3000, 2017.

710 Horrevoets, A. C., Savenije, H. H. G., Schuurman, J. N., and Graas, S.: The influence  
711 of river discharge on tidal damping in alluvial estuaries, *J. Hydrol.*, 294, 213-228,  
712 <https://doi.org/10.1016/j.jhydrol.2004.02.012>, 2004.

713 Hecht, J.S., Lacombe, G., Arias, M.E., Duc Dang, T. and Piman, T.: Hydropower  
714 dams of the Mekong River basin, a review of their hydrological impacts, *J. Hydrol.*,  
715 45(10): W10420, <https://doi.org/10.1016/j.jhydrol.2018.10.045>, 2018.

716 Huang, K., Ye, L., Chen, L., Wang, Q., Dai, L., Zhou, J., Singh, V. P., Huang, M., and  
717 Zhang, J.: Risk analysis of flood control reservoir operation considering multiple  
718 uncertainties, *J. Hydrol.*, 565, 672-684, <https://doi.org/10.1016/j.jhydrol.2018.08.040>,  
719 2018.

720 Kuang, C., Chen, W., Gu, J., Su, T. C., Song, H., Ma, Y., and Dong, Z.: River  
721 discharge contribution to sea-level rise in the Yangtze River Estuary, China, *Cont.*  
722 *Shelf Res.*, 134, 63-75, <https://doi.org/10.1016/j.csr.2017.01.004>, 2017.

723 Kosuth, P., Callède, J., Laraque, A., Filizola, N., Guyot, J.L., Seyler, P., Fritsch, J.M.,  
724 and Guimarães, V.: Sea-tide effects on flows in the lower reaches of the Amazon  
725 River, *Hydrol. Process.*, 23(22), 3141-3150, <https://doi.org/10.1002/hyp.7387>, 2009.

726 Liu, F., Hu, S., Guo, X., Cai, H., Yang, Q.: Recent changes in the sediment regime of  
727 the Pearl River (South China), Causes and implications for the Pearl River Delta,  
728 *Hydrol. Process.*, 32(12): 1771-1785, <https://doi.org/10.1002/hyp.11513>, 2018.

729 Lu, S., Tong, C., Lee, D.Y., Zheng, J., Shen, J., Zhang, W., and Yan, Y.: Propagation  
730 of tidal waves up in Yangtze Estuary during the dry season, *J. Geophys. Res.*, 120(9),  
731 6445-6473, <https://doi.org/10.1002/2014JC010414>, 2015.

732 Lu, X.X., Yang, X., and Li, S.: Dam not sole cause of Chinese drought, *Nature*  
733 475(7355), 174, <https://doi.org/10.1038/475174c>, 2011.

734 Lyu, Y., Zheng, S., Tan, G. and Shu, C.: Effects of Three Gorges Dam operation on  
735 spatial distribution and evolution of channel thalweg in the Yichang-Chenglingji  
736 Reach of the Middle Yangtze River, China, *J. Hydrol.*, 565, 429-442,  
737 <https://doi.org/10.1016/j.jhydrol.2018.08.042>, 2018.

738 Mei, X., Dai, Z., Gelder, P.H.A.J. and Gao, J.: Linking Three Gorges Dam and  
739 downstream hydrological regimes along the Yangtze River, China, *Earth Space Sci.*,  
740 2(4), 94-106, <https://doi.org/10.1002/2014EA000052>, 2015a.

741 Mei, X., Dai, Z., Du, J. and Chen, J.: Linkage between Three Gorges Dam impacts  
742 and the dramatic recessions in China's largest freshwater lake, Poyang Lake, *Sci. Rep.*,  
743 5,18197, <https://doi.org/10.1038/srep18127>, 2015b.

744 Nakayama, T., and Shankman, D.: Impact of the Three-Gorges Dam and water  
745 transfer project on Changjiang floods, *Global Planet Change*, 100, 38-50,  
746 <https://doi.org/10.1016/j.gloplacha.2012.10.004>, 2013.

747 Qiu, C. and Zhu., J.: Influence of seasonal runoff regulation by the Three Gorges  
748 Reservoir on saltwater intrusion in the Changjiang River Estuary, *Cont. Shelf Res.*, 71,  
749 16-26, <https://doi.org/10.1016/j.csr.2013.09.024>, 2013.

750 Rahman, M., Dustegir, M., Karim, R., Haque, A., Nicholls, R. J., Darby, S. E.,  
751 Nakagawa, H., Hossain, M., Dunn, F. E., and Akter, M.: Recent sediment flux to the  
752 Ganges-Brahmaputra-Meghna delta system, *Sci. Total Environ.*, 643, 1054-1064,  
753 <https://doi.org/10.1016/j.scitotenv.2018.06.147>, 2018.

754 Räsänen, T. A., Someth, P., Lauri, H., Koponen, J., Sarkkula, J., and Kummu, M.:  
755 Observed river discharge changes due to hydropower operations in the Upper Mekong  
756 Basin, *J. Hydrol.*, 545, 28-41, <https://doi.org/10.1016/j.jhydrol.2016.12.023>, 2017.

757 Sassi, M. G., and Hoitink, A. J. F.: River flow controls on tides and tide-mean water  
758 level profiles in a tidal freshwater river, *J. Geophys. Res.*, 118(9), 4139-4151,  
759 <https://doi.org/10.1002/jgrc.20297>, 2013.

760 Savenije, H. H. G.: *Salinity and Tides in Alluvial Estuaries*, Elsevier, New York, USA,  
761 2005.

762 Savenije, H. H. G.: *Salinity and Tides in Alluvial Estuaries* (2nd completely revised  
763 edition), Available at [www.salinityandtides.com](http://www.salinityandtides.com) (Last access: 10 December 2018),  
764 2012.

765 Savenije, H. H. G., Toffolon, M., Haas, J., and Veling, E. J. M.: Analytical description  
766 of tidal dynamics in convergent estuaries, *J. Geophys. Res.*, 113, C10025,  
767 <https://doi.org/10.1029/2007JC004408>, 2008.

768 Shaikh, B.Y., Bansal, R.K., Das, S.K.: Propagation of Tidal Wave in Coastal Terrains  
769 with Complex Bed Geometry, *Environmental Processes*, 5(3), 519-537,  
770 <https://doi.org/10.1007/s40710-018-0314-7>, 2018.

771 Shi, S., Cheng, H., Xuan, X., Hu, F., Yuan, X., Jiang, Y., and Zhou, Q.: Fluctuations in  
772 the tidal limit of the Yangtze River estuary in the last decade, *Sci. China Earth*  
773 *Sci.*, 61 (8), 1136-1147, <https://doi.org/10.1007/s11430-017-9200-4>, 2018.

774 Wang, Y., Ridd, P.V., Wu, H., Wu, J. and Shen, H.: Long-term morphodynamic  
775 evolution and the equilibrium mechanism of a flood channel in the Yangtze Estuary

776 (China), *Geomorphology*, 99(1-4), 130-138, [https://doi.org/10.1016/j.geomorph.](https://doi.org/10.1016/j.geomorph.2007.10.003)  
777 2007.10.003, 2008.

778 Vignoli, G., Toffolon, M., and Tubino, M.: Non-linear frictional residual effects on  
779 tide propagation, in, *Proceedings of IAHR Congress*, vol. A, 24-29 August 2003,  
780 Thessaloniki, Greece, 291-298, 2003.

781 Zhang, E. F., Savenije, H. H. G., Chen, S. L., and Mao, X. H.: An analytical solution  
782 for tidal propagation in the Yangtze Estuary, China, *Hydrol. Earth Syst. Sci.*, 16(9),  
783 3327-3339, <https://doi.org/10.5194/hess-16-3327-2012>, 2012.

784 Zhang, F., Sun, J., Lin, B., and Huang, G.: Seasonal hydrodynamic interactions  
785 between tidal waves and river flows in the Yangtze Estuary, *J. Marine Syst.*, 186,  
786 17-28, <https://doi.org/10.1016/j.jmarsys.2018.05.005>, 2018.

787 Zhang, M., Townend, I., Cai, H., and Zhou, Y.: Seasonal variation of tidal prism and  
788 energy in the Changjiang River estuary: A numerical study, *Chin. J. Oceanol. Limn.*,  
789 34 (1), 219-230, <https://doi.org/10.1007/s00343-015-4302-8>, 2015a.

790 Zhang, M., Townend, I., Cai, H., and Zhou, Y.: Seasonal variation of river and tide  
791 energy in the Yangtze estuary, China, *Earth Surf. Proc. Land.*, 41(1): 98-116,  
792 <https://doi.org/10.1002/esp.3790>, 2015b.

793 Zhao, T., Zhao, J., Yang, D. and Wang, H.: Generalized martingale model of the  
794 uncertainty evolution of streamflow forecasts, *Adv. Water Resour.*, 57, 41-51,  
795 <https://doi.org/10.1016/j.advwatres.2013.03.008>, 2013.

796

797 **Appendix A. Simplified momentum balance for the residual water level slope**

798 Assuming a periodic variation of flow velocity, the integration of Equation (1)(1)(1)  
 799 over a tidal cycle leads to an expression for the residual water level slope (e.g. Cai et  
 800 al., 2014a, 2016):

$$801 \quad \frac{\partial \bar{Z}}{\partial x} = -\frac{1}{K^2} \left( \frac{\overline{U|U|}}{h^{4/3}} \right) - \frac{1}{2g} \frac{\partial \overline{U^2}}{\partial x} - \frac{1}{2\rho_0} h \frac{\partial \bar{\rho}}{\partial x} \quad (8)$$

802 where the overbars and the subscript 0 indicate the tidal average and value at the  
 803 seaward boundary, respectively. The residual water level slope is induced by three  
 804 contributions: residual frictional, advective acceleration, and density effects, which  
 805 correspond to the three terms on the right-hand side of Equation (8)(8)(8). Note that  
 806 the contribution from advective acceleration to the residual water level slope:

$$807 \quad \frac{\partial \bar{Z}_{adv}}{\partial x} = -\frac{1}{2g} \frac{\partial \overline{U^2}}{\partial x}, \quad (9)$$

808 can be easily integrated to:

$$809 \quad \bar{Z}_{adv} = -\frac{1}{2g} (\overline{U^2} - \overline{U_0^2}) = -\frac{1}{2} Fr_0 \left( \frac{\overline{U^2}}{\overline{U_0^2}} - 1 \right) \bar{h}_0 \quad (10)$$

810 where the Froude number is introduced,  $\overline{Fr^2} = \overline{U^2}/(g\bar{h})$ , which is computed with  
 811 the averaged variables. In this case, the correction is local (not cumulative) and  
 812 proportional to the flow depth through a coefficient that is negligible as long as the  
 813 velocity does not change significantly, and  $Fr$  is small, as is common in most tidal  
 814 flows. It was shown by Savenije (2005, 2012) that the density term in equation  
 815 (1)(1)(1) always exercises a pressure in the landward direction, which is counteracted  
 816 by a residual water level slope, amounting to 1.25% of the estuary depth over the salt  
 817 intrusion length. The value for the residual water level slope, induced by the density  
 818 effect, is usually small compared with the gradient of the free surface elevation; thus,

设置了格式: 字体颜色: 文字 1

设置了格式: 字体颜色: 文字 1

819 in this paper, we neglect the influence of the density difference on the dynamics of the  
 820 residual water level.

821

## 822 **Appendix B. Governing equations for tide-river dynamics in estuaries**

823 The analytical solutions for the dependent parameters  $\mu$ ,  $\delta$ ,  $\lambda$ , and  $\varepsilon$  are obtained by  
 824 solving the following four dimensionless equations (see details in Cai et al., 2014a):

825 the tidal damping/amplification equation, describing the tidal amplification or  
 826 damping as a result of the balance between channel convergence ( $gq$ ) and bottom  
 827 friction ( $cm/G$ ):

$$828 \quad \delta = \frac{\mu^2 (\gamma\theta - \chi\mu\lambda\Gamma)}{1 + \mu^2\beta}, \quad (11)$$

829 the scaling equation, describing how the ratio of velocity amplitude to tidal amplitude  
 830 depends on phase lag and wave celerity:

$$831 \quad \mu = \frac{\sin(\varepsilon)}{\lambda} = \frac{\cos(\varepsilon)}{\gamma - \delta}, \quad (12)$$

832 the celerity equation, describing how the wave celerity depends on the balance  
 833 between convergence and tidal damping/amplification:

$$834 \quad \lambda^2 = 1 - \delta(\gamma - \delta), \quad (13)$$

835 and the phase lag equation, describing how the phase lag between HW and HWS  
 836 depends on wave celerity, convergence, and damping:

$$837 \quad \tan(\varepsilon) = \frac{\lambda}{\gamma - \delta}, \quad (14)$$

838 where  $q$ ,  $b$ , and  $G$  account for the effect of river discharge and where:

$$839 \quad \beta = \theta - r_s \zeta \varphi / (\mu\lambda), \quad \theta = 1 - (\sqrt{1 + \zeta} - 1) \varphi / (\mu\lambda), \quad \Gamma = \frac{1}{\pi} [p_1 - 2p_2\varphi + p_3\varphi^2 (3 + \mu^2\lambda^2 / \varphi^2)].$$

840 (15)

841 Note that  $\Gamma$  is a friction factor obtained by using Chebyshev polynomials (Dronkers,  
 842 1964) to represent the non-linear friction term in the momentum equation:

$$843 \quad F = \frac{U|U|}{K^2 h^{-4/3}} \approx \frac{1}{K^2 h^{-4/3} \pi} (p_0 v^2 + p_1 vU + p_2 U^2 + p_3 U^3 / v) \quad (16)$$

844 in which  $U$  is the cross-sectional averaged velocity consisting of a steady component  
 845  $U_r$ , generated by the fresh water discharge, and a time-dependent component  $U_t$ ,  
 846 introduced by the tide:

$$847 \quad U = U_t - U_r = v \sin(\omega t) - Q / \bar{A} \quad (17)$$

848 where  $Q$  is the fresh water discharge (treated as a constant during the tidal wave  
 849 propagation), and  $p_i$  ( $i=0, 1, 2, 3$ ) are the Chebyshev coefficients (see Dronkers,  
 850 1964, p. 301), which are functions of the dimensionless river discharge  $\varphi$  through  
 851  $\alpha = \arccos(-\varphi)$ :

$$852 \quad p_0 = -\frac{7}{120} \sin(2\alpha) + \frac{1}{24} \sin(6\alpha) - \frac{1}{60} \sin(8\alpha), \quad (18)$$

$$853 \quad p_1 = \frac{7}{6} \sin(\alpha) - \frac{7}{30} \sin(3\alpha) - \frac{7}{30} \sin(5\alpha) + \frac{1}{10} \sin(7\alpha), \quad (19)$$

$$854 \quad p_2 = \pi - 2\alpha + \frac{1}{3} \sin(2\alpha) + \frac{19}{30} \sin(4\alpha) - \frac{1}{5} \sin(6\alpha), \quad (20)$$

$$855 \quad p_3 = \frac{4}{3} \sin(\alpha) - \frac{2}{3} \sin(3\alpha) + \frac{2}{15} \sin(5\alpha). \quad (21)$$

856 The coefficients  $p_1$ ,  $p_2$ , and  $p_3$  determine the magnitudes of the linear, quadratic, and  
 857 cubic frictional interaction, respectively.

858